UNIVERSITY OF CALIFORNIA, SAN DIEGO

# Development of Biochemical Profile of Novel Bigenic Mouse AD Model

A thesis submitted in partial satisfaction of the

requirements for the degree Master of Science

in

Biology

by

Andrew Arner

Committee in charge:

Professor Gentry Patrick, Chair
Professor Robert Rissman, Co-Chair
Professor Randy Hampton

2016

The thesis of Andrew Arner is approved and it is acceptable in quality and form for publication on microfilm and electronically:

---

---

Co-Chair

---

Chair

University of California, San Diego

2016

TABLE OF CONTENTS

LIST OF TABLES AND FIGURES

# ACKNOWLEDGEMENTS

I would like to thank Dr. Robert Rissman for his mentorship and constant guidance during the work that I have done over the past two years. I would also like to acknowledge Dr. Gentry Patrick and Dr. Randy Hampton for being members of my committee.

I would like to thank Dr. Eliezer Masliah, for giving me this project and providing me with the lab equipment, reagents, and tissue needed to conduct the research of this project. I would like to extend my appreciation to Ed Rockenstein for engineering and providing me with the mice that were used for all of the data involved.

The Results Section is currently being prepared for submission for publication of the material as it appears in "Development of Biochemical Profile of Novel Bigenic Mouse AD Model", Arner, Andrew; Adame, Adam. Andrew Arner was the primary investigator and author of this material.

ABSTRACT OF THE THESIS

Development of Biochemical Profile of Novel Bigenic Mouse AD Model

by

Andrew Arner

Master of Science in Biology

University of California, San Diego, 2016

Professor Gentry Patrick, Chair

Professor Robert Rissman, Co-Chair

Tauopathies encompass several of the most prevalent neurodegenerative diseases that consistently progress to severe dementia and motor impairments. They

involve tau hyperphosphorylation, which leads to the proteins detachment from associated microtubules, and a decline in the structural integrity of the cytoskeleton. This disassociation is followed by intracellular tau aggregation that causes impairment of axonal function. The most common tauopathy, Alzheimer disease (AD), affects 5 million individuals in the United States alone. Due to a lack of understanding of the pathology involved in AD, treatment is currently limited to minimizing symptoms, without the ability to slow the rate of neurodegeneration. Another component of AD is that it is uniquely associated with extracellular accumulation of amyloid beta plaques, which appear to disrupt synaptic function, as well as induce inflammation. Developing and researching a variety of transgenic animals meant to model these diseases is critical to advancing the efficacy of their treatment and prevention. A line of transgenic mice containing the human amyloid precursor protein gene (hAPP) was bred with a recently generated line of mice that overexpress a variant of the human triple repeat tau gene, to create a novel bigenic line of mice that model AD. A biochemical and cognitive profile was developed for both young and aged mice with these three differing transgenic genotypes, along with a control group of non-transgenic mice.

# INTRODUCTION

The microtubule associated protein tau (MAPT) gene is present in a variety of animal species, present in chromsome 17 in humans, and encodes for a transcript that is spliced into several isoforms, ranging from 352 to 441 amino acid residues. The six isoforms expressed in the human brain differ in their absence or presence of one or two 29 amino acid residues in the amino-terminal, as well as their presence of three (3RTau) or four (4RTau) microtubule binding repeat segments, each with 31 residues, in the carboxy-terminal [1]. The three-repeat tau isoform without any N-terminal inserts (3R0N) is the only isoform expressed in the embryonic brain of mammals, while only the four-repeat (4RTau) isoforms are found in the postnatal mouse brain [2]. This differs from the expression in the adult human brain, which includes all six isoforms. While 3RTau has been shown to have a lower affinity for microtubules than 4RTau, studies reveal that this has little to do with the additional C-terminal segment in 4RTau, and that both forms contain a microtubule binding-domain, which incudes the initial two repeated C-terminal segments and the segment they flank [3]. In addition, both groups of isoforms display differential regulation in their microtubule binding, for example, C-terminal and N-terminal sequences in the 3RTau isoforms have been shown to be relevant for such regulation, while 4Rtau microtubule affinity lacks such association [4].

There are 40 phosphorylation sites that have ben identified in tau protein isolated from AD brains, several of which including Ser262, Thr231 and Ser235 are found to be associated with inhibition of the proteins potential to bind to microtubules; while phosphorylation at other sites, such as Ser396, promotes self-aggregation [5]. There

is also evidence that the rate of tau phosphorylation from some of its common kinases, such as Cdk5 and Gsk3-β, increases after a certain level of initial phosphorylation occurs [6]. These aggregates then form intracellular tangles of paired helical filaments (PHF) that then constitute neurofibrillary tangles (NFTs), a defining characteristic of tauopathies, which disrupt neuronal function. The damage of these occurrences is twofold; the NFTs obstruct axonal transport, while the microtubules are less stable without the normal amount of tau present in their structure. A curious finding is that the ratio of the presence of hyperphosphorylated 4RTau and 3RTau aggregates in the human adult brain has been correlated with the specific type of tauopathy present in the diseased brain, with much lower phosphorylation and a 1:1 expression rate of the isoforms in healthy human brains [7]. Common tauopathy examples are: AD brains containing close to a 1:1 ratio, the 3RTau isoforms predominating in Picks diseased (PiD) brains, and the 4RTau isoforms up-regulated in the brains of patients suffering from progressive supranuclear palsy (PSP), corticobasal degeneration (CBD) and frontotemporal dementia with parkinsonism-17 (FTDP-17)[8].

The extracellular aggregation of Amyloid-Beta (Aβ) plaques is a second hallmark of AD. Particularly the 42 amino acid peptide cleaved from the amyloid precursor protein (APP), which has shown to be colocalized with neuronal death, thus leading to the 'amyloid hypothesis' [9]. Interestingly, the level tau NFTs alone, but not the amyloid plaques alone, have been positively correlated with the severity of dementia in AD patients [10]. This then leads to the belief that amyloid plaques cause additional neurological harm only when an abundance of NFTs are also present. It is worth noting,

however, that the presence of Aβ plaques and their role is somewhat obscure, as several studies have found a potential neuroprotective effect of the aggregates as an antioxidant, an excitotoxic inhibitor [11], as well as an antibiotic [12].

## MATERIALS AND METHODS

### Generation of mThy-1 3R Tau mutant transgenic mice and treatments.

All experiments were approved by the University of California San Diego's animal subjects committee. The mice carrying the mutated human 3RTau gene associated with familial PiD, L266V and G272V, that was generated under the neuronal mThy-1 promoter cassette (provided by Dr. H. van der Putten) were generated in the C57BL/6 background as previously described [11]. Line 13, the higher expressing line of mice were chosen. Several were crossed with Line 41 mutated human APP mice (K670N/761NL and V717I), also under the mThy-1 promoter cassette. Mice were divided into young (3 months) and aged (6 months) to elucidate the long-term effects of Aβ plaques.

### Tissue preparation

After collecting behavioral data, mice were sacrificed following NIH guidelines. The right hemi-brain was post-fixed for 48 hours in 4% phosphate-buffered paraformaldehyde (pH 7.4) at 4°C and sagittal sectioned Vibratome 2000 (40 $\mu$m; Leica, Deerfield, IL). The left hemibrain was snap-frozen and stored at –70°C.

### Immunohistochemistry and image analysis

The level of tau expression was detected using free-floating, blind-coded vibratome (50 $\mu$m) sections. The sections were then incubated with antibodies against 3R Tau (1:250, Millipore) and pTau (PHF-1; 1:500, gift from Peter Davies) overnight at 4°C. They were

then incubated in biotin-tagged IgG1 secondary antibodies (1:100, Vector Laboratories, Inc., Burlingame, CA), or Avidin D-HRP (1:200, ABC Elite, Vector), and visualized with diaminobenzidine. A digital Olympus bright field digital microscope (BX41) was used to scan the sections.

Neuropathology was quantified by incubating the sections overnight at 4°C in antibodies against the astroglial marker; glial fibrillary acidic protein (GFAP, 1:1000, Millipore) and the neuronal marker NeuN (1:500, Millipore). These sections were then incubated with secondary antibodies, Avidin D-HRP, and visualized with diaminobenzidine. The levels of Tau and GFAP were analyzed in layer 5 of the neocortex, in the hippocampus dentate gyrus and area CA1 with Image J and expressed as optical density. Four images were capture for each section at 400X and converted to gray scale, opened with Image J, thresholded and a dynamic scale set to determine optical density. The number of neurons immunoreactive with NeuN were estimated using unbiased stereological methods {Overk, 2008 #10028}. Sections of the hemibrain containing the hippocampus, striatum, and neocortex were outlined using an Olympus BX51 microscope running StereoInvestigator 8.21.1 software (Micro-BrightField, Cochester, VT). Grid size for the dentate gyrus was: 300×300 $\mu$m, and the counting frame was 50×50 $\mu$m. The average coefficient of error for each region was 0.09. Sections were analyzed using a 100×1.4 PlanApo oil-immersion objective. A 5 $\mu$m high dissector, allowed for 2 $\mu$m top and bottom guard-zones.

**Tissue fractionation and immunoblot analysis.**

Frozen samples of the posterior half of the right mouse hemibrain, that includes the neocortex and hippocampus, were homogenized in detergent-containing 12% phosphatase inhibitors, and 12% protease inhibitors in PDGF lysis buffer. Homogenates were separated into soluble and insoluble fractions through centrifugation at 100,000 g for 60 minutes. A BCA assay was used to analyze the samples; protein (20 $\mu$g/lane) was loaded into each well of a 4-12% SDS-PAGE gel and run in 5% MES (20X) running buffer at 200 V for 50 minutes. The gels were then blotted onto a nitrocellulose membrane, using Thermo Fisher iBlot 2 western detection stacks. Blots were incubated for detection of specific target proteins using the corresponding antibody listed in Table 1 for two days at 4 °C. The membrane was then washed and incubated in horseradish-peroxidase-conjugated secondary antibody of the appropriate species (1:1000 Santa Cruz Biotechnology) for 60 minutes at room temperature. Bands were then washed and visualized by enhanced chemiluminescence (ECL, PerkinElmer, Boston, MA) and analyzed with a quantitative Versadoc XL imaging apparatus (BioRad, Hercules, CA) and analyzed with Quantity One Software. β-Actin (1:3,000, Sigma Aldrich) was used as the loading control.

**Table 1:** List of specific antibodies used for immunohistochemistry and immunoblotting.

| Antibody | Immunogen | Specificity | Source | Host | Application |
|---|---|---|---|---|---|
| p35 | C-19 | Mouse, human | S.B.C., sc-820 | Rabbit, polyclonal | WB, IP, IF, ELISA |
| CDK5 | Human CDK5 (C-8) | Mouse, human | S.B.C., sc-173 | Rabbit, polyclonal | WB, IP, IF, ELISA |
| GSK-3β | Human GSK-3β (27C10) | Primates, mouse | Cell-Sig., #9315 | Rabbit monoclonal | WB, IP, IHC |
| p-GSK-3β | Phopsho peptide $Y^{216}$ | Mouse, human | S.B.C., sc-135653 | Rabbit polyclonal | WB, IP, IF, IHC |
| Total Tau | Tau, 210-241 | Human, Mouse | Millipore, MAB361 | Mouse monoclonal | IHC, WB |
| PHF-1 | Tau pSer202 + Thr205 | Multiple species | Thermo-S., MN1020 | Mouse monoclonal | WB, IF, IHC, ELISA |
| β-Actin | β-Actin (N-Terminal) | Multiple species | Sig.-Ald., A5316 | Mouse monoclonal | WB, IHC, IF |
| 3R Tau | Tau, 3-repeat isoform | Human, mouse, | Millipore, 05-804 | Mouse monoclonal | IHC, WB |
| 82E1 | Human Amyloid-β | Human, mouse | I.B.L-CN. 10323 | Mouse monoclonal | IP, WB, IHC |
| GFAP | Glial Fibrillary Acidic Protein | Multiple Species | Millipore, MAB360 | Mouse monoclonal | ICC, IP, IHC, WB |
| NeuN | NeuN Protein | Multiple Species | Millipore, MAB377 | Mouse monoclonal | IF, IHC, WB, ICC, IP |

**Statistical analysis**

GraphPad 5.0 was used for all analyses. One-way ANOVA was used to assess the differences among means with Dunnett's post-hoc test when compared to non-tg and by Tukey-Kramer when comparing tg groups. Two-way ANOVA with repeated measures followed by a Bonferroni multiple comparisons post-hoc test was used for analyzing the interactions between groups and time. The null hypothesis was rejected at the 0.05 level.

## RESULTS

### Overexpression of APP/Ab in 3RTau transgenic mice results in increased tau accumulation and phosphorylation in IHC sections

To compare the effects of mice carrying mutant hAPP, mutant 3RTau, or both with non-tg mice, we studied both 3 month and 6 month old mice. The young APP and non-tg mice showed lower levels of 3RTau immunoreactivity compared with the 3RTau and APP-3RTau mice in both the neocortex (Figure 1a, b) and hippocampus (Figure 1a-d), with 3RTau aggregates mostly in pyramidal neurons and in the granular cells in the dentate gyrus (Figure 1a). Similar levels of 3RTau were detected in the CA1 region of the hippocampus for both young mice lines carrying 3RTau (Figure 1a, d), however there were higher levels of the tau isoform found in the APP-3RTau mice in the neocortex (Figure 1a, b) and dentate gyrus (Figure 1a, c).

Similarly, in the aged group, higher levels of 3R Tau immunoreactivity was found in the APP-3RTau mice than the single tg 3RTau mice in the dentate gyrus (Figure 1e, g) and CA1 region of the hippocampus (Figure 1e, h), with an insignificant trend found in the neocortex (Figure 1e, f). Of course, both of these lines showed higher levels of 3RTau than the APP and non-tg mice in all regions observed (Figure 1e).

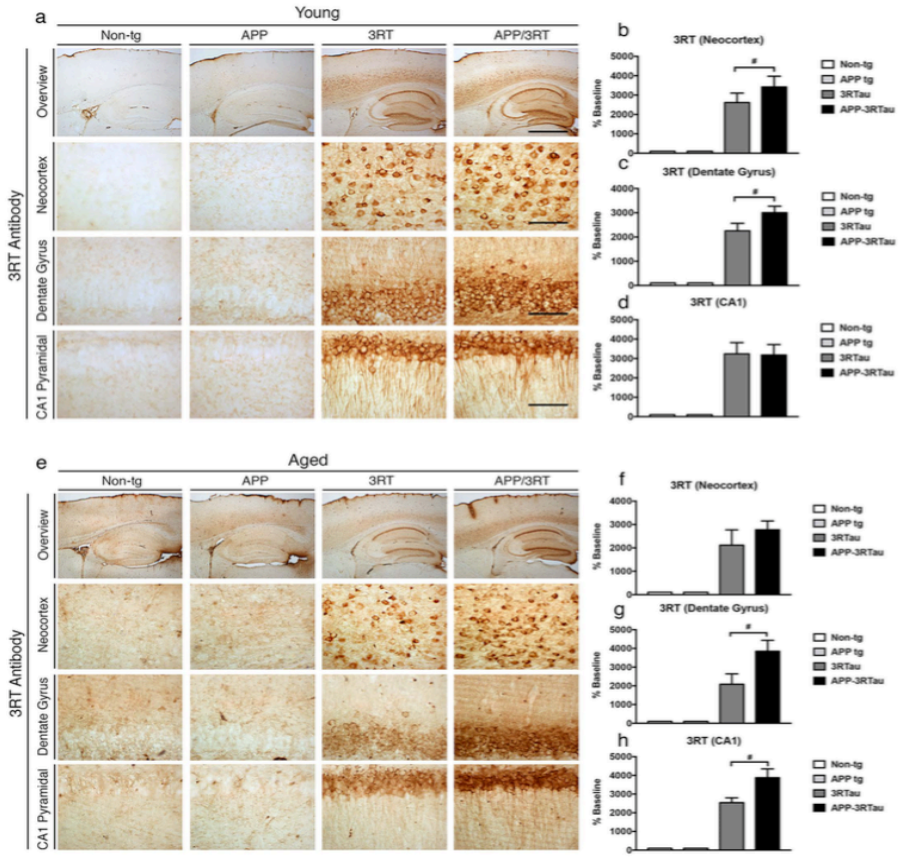


**Figure 1: Pattern of 3RTau distribution in the brains of the three lines of mice compared with the non-tg control. A** Immunostaining with an antibody against 3R Tau was used on vibratome sections of the young mice, followed by analysis by digital bright field microscopy. Panels on the top row are low-magnification (40X) photomicrographs of the neocortex and hippocampus. The lower three rows of panels are higher magnification (630X) of the corresponding regions. **B** Image analysis of number of neuronal cells in the neocortex, **C** dentate gyrus, and **D** CA1 hippocampus region displaying 3R Tau aggregates. **E** Immunostaining with an antibody against 3RTau was used on vibratome sections of the aged mice, followed by analysis by digital bright field microscopy. Panels on the top row are low-magnification (40X) photomicrographs of the neocortex and hippocampus. The lower three rows of panels are higher magnification (630X) of the corresponding regions. **F** Image analysis of number of neuronal cells in the neocortex, **G** dentate gyrus, and **H** CA1 hippocampus region displaying 3RTau aggregates. # = $P < 0.05$ when comparing the three lines of transgenic mice with one another using a one way ANOVA with Tukey-Kramer post-hoc test.

Next, to assess any effects carrying both genes may have on tau phosphorylation we performed immunohistochemical analysis using an anti-PHF-1 antibody. For the young mice compared to non-tg controls, that APP mice showed a slight increase in PHF-1 levels (Figure 2a), while the 3RTau and APP-3RTau mice displayed significant increases in immunoreactivity in the neocortex (Figure 2a, b) and hippocampus (Figure 2a-d), with the aggregates mainly localized to the pyramidal neurons in the neocortex and hippocampus (Figure 2a). Increased amounts of phosphorylated tau were found in young APP-3RTau mice when compared to the 3RTau mice in the neocortex (Figure 2a, b), dentate gyrus (Figure 2a, c) and region CA1 of the hippocampus (Figure 2a, d).

A similar trend was found for the aged mice with slightly higher levels of PHF-1 in the APP mice when compared to the non-tg mice (Figure 2e), while both mice lines with the 3RTau gene displayed significantly higher levels in the three observed areas (2e, f-h). Again the APP-3RTau mice showed more immunoreactivity in the CA1 region of the hippocampus than did the 3RTau mice (Figure 2e, h). Together, these results suggest that there is an increase in tau aggregation/phosphorylation in 3RTau mice that overexpress APP.

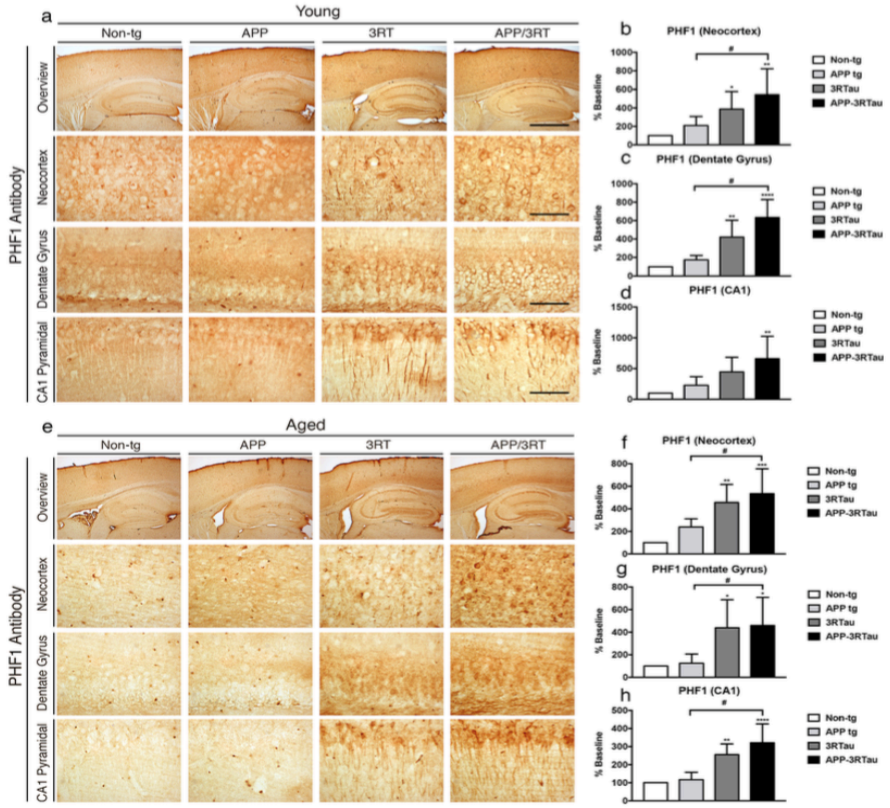


**Figure 2: Pattern of pTau distribution in the brains of the three lines of mice compared with the non-tg control.** A Immunostaining with a PHF-1 antibody was used on vibratome sections of the young mice against pTau (Ser396 and Ser404), followed by analysis by digital bright field microscopy. Panels on the top row are low-magnification (40X) photomicrographs of the neocortex and hippocampus. The lower three rows of panels are higher magnification (630X) of the corresponding regions. **B** Image analysis of number of neuronal cells in the neocortex, **C** dentate gyrus, and **D** CA1 hippocampus region displaying pTau aggregates. **E** Immunostaining with a PHF-1 antibody was used on vibratome sections of the young mice against pTau (Ser396 and Ser404), followed by analysis by digital bright field microscopy. Panels on the top row are low-magnification (40X) photomicrographs of the neocortex and hippocampus. The lower three rows of panels are higher magnification (630X) of the corresponding regions. **F** Image analysis of number of neuronal cells in the neocortex, **G** dentate gyrus, and **H** CA1 hippocampus region displaying pTau aggregates. *,**,***,**** = $P < 0.05, 0.01, 0.001, 0.0001$, respectively, when compared to non-tg control using one way ANOVA with Dunnett's post-hoc test. # = $P < 0.05$ when comparing the three lines of transgenic mice with one another using a one way ANOVA with Tukey-Kramer post-hoc test.

**Immunoblot analysis of levels of 3RTau and p-Tau in double transgenic APP-3RTau mice**

Antibodies specific for the 3RTau isoform revealed that only the two lines mice carrying the 3RTau transgene had detectable levels of the protein, in both the soluble and insoluble fractions of both ages (Figure 3a, b, f, g and Figure 4a, b, f, g). The 3RTau levels were found to be significantly higher in the 3RTau mice when compared with the APP-3RTau mice in all ages and fractions excluding the young soluble fraction, where the levels were not significantly different. The PHF1 antibody revealed significantly higher levels of phosphorylated tau in the 3RTau mice, with significantly increased levels in the APP-3RTau mice in the soluble fraction for the aged mice (Figure 3f, h). A similar pattern seems to emerge for the insoluble fraction of the aged mice, but like both fractions of the young mice, the differences were not proven to be statistically significant (Figure 3a, c, and Figure 4a, c, f, h). The two lines of mice of both ages carrying the 3RTau transgene displayed higher levels of total tau, compared to the APP and non-tg mice, when an antibody used to detect each isoform of tau was used (Figure 3a, d, f, i and Figure 4a, d, f, i). An antibody specific for Ab detected both tetramer and monomer levels in the only the insoluble fraction of both ages for the APP and APP-3Rtau mice (Figure 3a, e, f, j and Figure 4a, e, f, j).

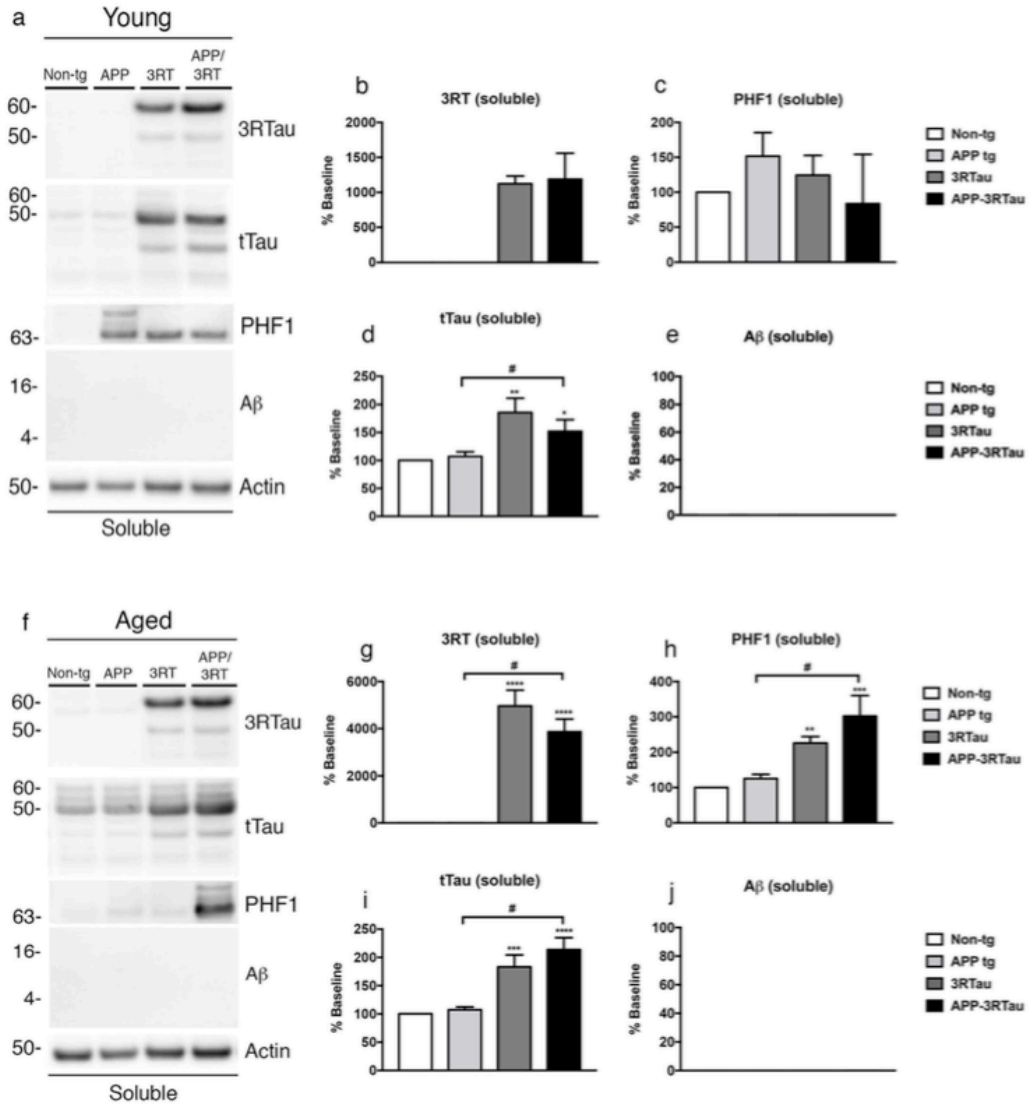


**Figure 3: Western blot analyses of the hemibrain of the APP-3RTau, APP, 3RTau and non-tg mice. A** Representative Western blot (SDS) and analyses of levels of **B** 3RTau, **C** PHF1, **D** tTau, and **E** Ab from the soluble fraction of the young mice. **F** Representative Western blot (SDS) and analyses of levels of **G** 3RTau, **H** PHF1, **I** tTau, and **J** Ab from the soluble fraction of the aged mice. N = 3 for each age group *,**,***,**** = $P < 0.05, 0.01, 0.001, 0.0001$, respectively, when compared to non-tg control using one way ANOVA with Dunnett's post-hoc test. # = $P < 0.05$ when comparing the three lines of transgenic mice with one another using a one way ANOVA with Fisher's post-hoc test.

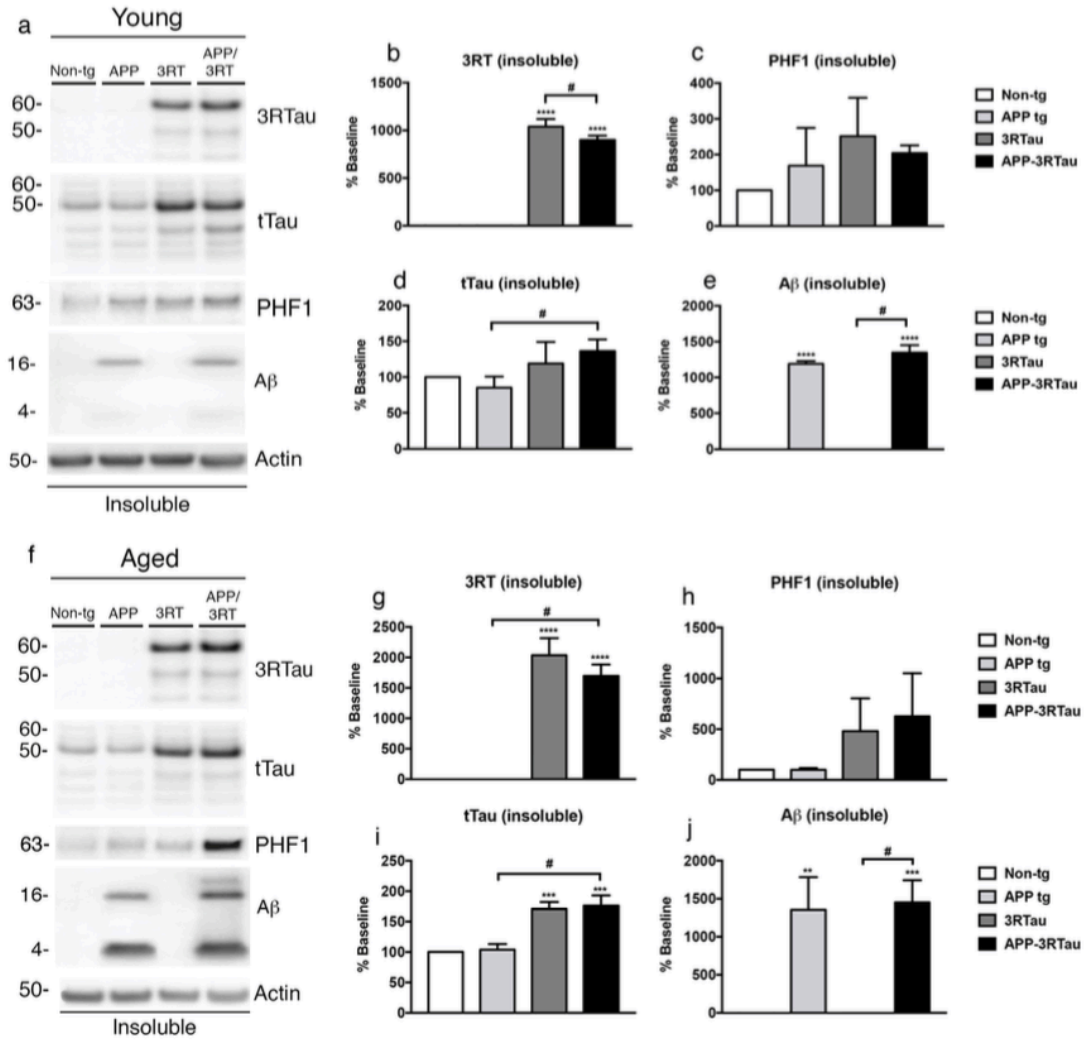


**Figure 4: Western blot analyses of the hemibrain of the APP-3RTau, APP, 3RTau and non-tg mice. A** Representative Western blot (SDS) and analyses of levels of **B** 3RTau, **C** PHF1, **D** tTau, and **E** Ab from the insoluble fraction of the young mice. **F** Representative Western blot (SDS) and analyses of levels of **G** 3RTau, **H** PHF1, **I** tTau, and **J** Ab from the insoluble fraction of the aged mice. N = 3 for each age group **,***,**** = $P < 0.01, 0.001, 0.0001$, respectively, when compared to non-tg control using one way ANOVA with Dunnett's post-hoc test. # = $P < 0.05$ when comparing the three lines of transgenic mice with one another using a one way ANOVA with Fisher's post-hoc test.

**Immunoblot analysis of levels of kinases involved in Tau phosphorylation in double transgenic APP-3RTau mice**

To further analyze the pathogenesis in pathways for tau and amyloid toxicity we targeted several kinases, their activated states, and some of their relevant activating proteins. Significant increases in the levels of both total GSK3 and its activated form, p-Y216, were found in the soluble fraction of the young 3RTau mice (Figure 5a, b, d). While Cdk5 levels were not found to differ between any of the lines of mice, its neuron-specific activator protein, p35, was found to be overexpressed in the soluble fraction of the young APP-3RTau mice (Figure 5a, c, e). Total GSK3 levels were detected at significantly higher levels for all transgenic models in the soluble aged fraction (5f, g).

As for the insoluble fractions of the same upstream proteins, total GSK3 was observed in higher levels for the young mice of the two lines carrying the 3RTau transgene (Figure 6a, b), as well as the aged APP mice, and decreased levels for the aged APP-3RTau mice (Figure 6f, g). All other results did not show significant deviation from the non-tg levels detected.

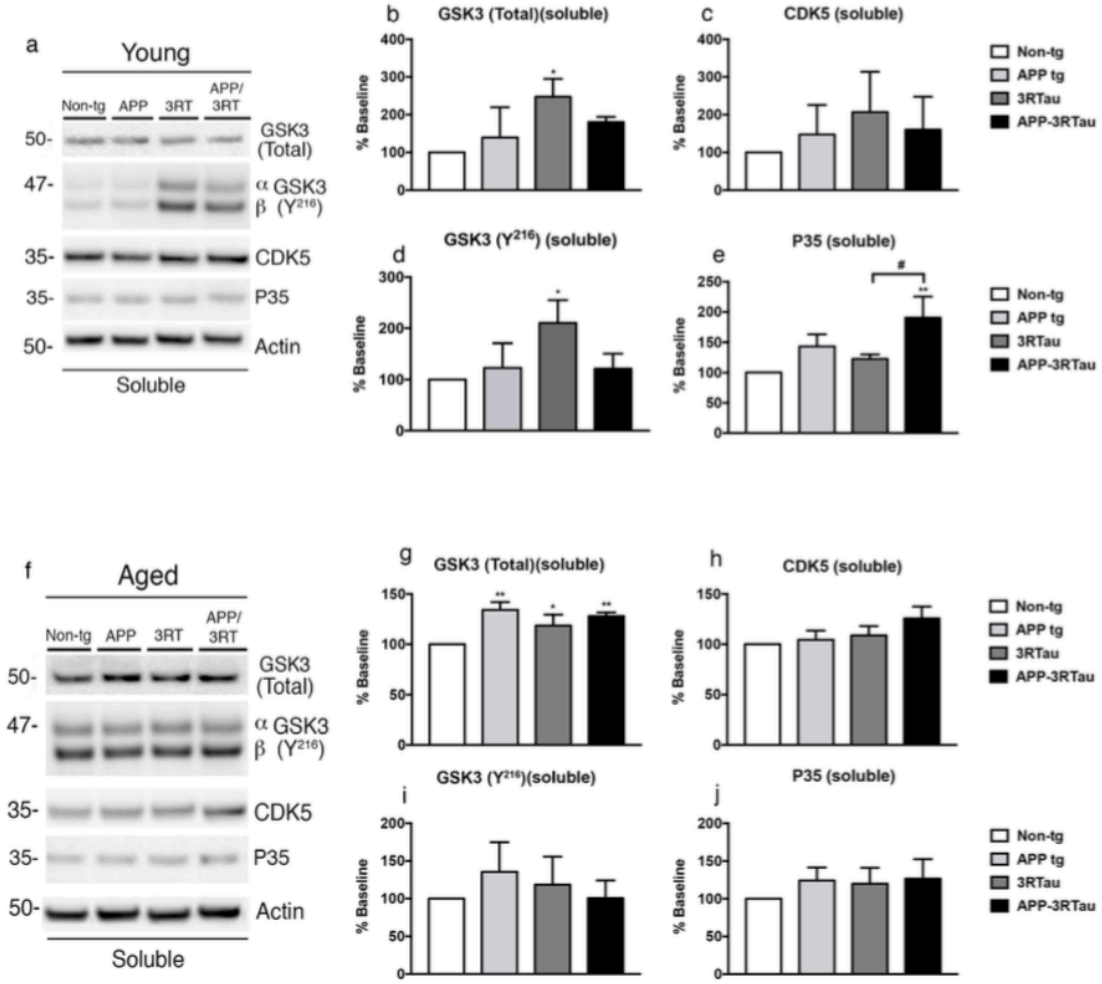


**Figure 5: Western blot analyses of the hemibrain of the APP-3RTau, APP, 3RTau and non-tg mice. A** Representative Western blot (SDS) and analyses of levels of **B** 3RTau, **C** PHF1, **D** tTau, and **E** Ab from the soluble fraction of the young mice. **F** Representative Western blot (SDS) and analyses of levels of **G** 3RTau, **H** PHF1, **I** tTau, and **J** Ab from the soluble fraction of the aged mice. N = 3 for each age group *,** = $P < 0.05, 0.01$, respectively, when compared to non-tg control using one way ANOVA with Dunnett's post-hoc test. # = $P < 0.05$ when comparing the three lines of transgenic mice with one another using a one way ANOVA with Fisher's post-hoc test.

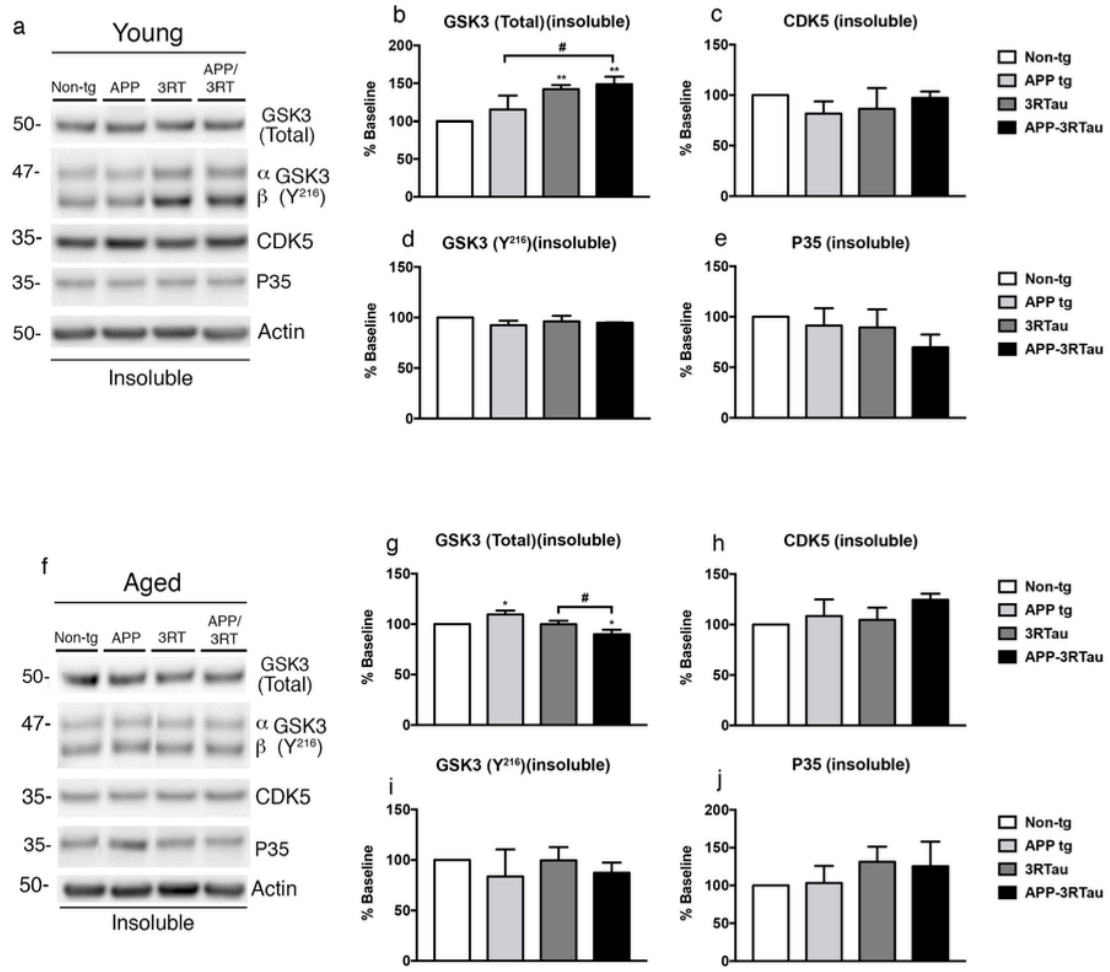


**Figure 6: Western blot analyses of the hemibrain of the APP-3RTau, APP, 3RTau and non-tg mice. A** Representative Western blot (SDS) and analyses of levels of **B** 3RTau, **C** PHF1, **D** tTau, and **E** Ab from the soluble fraction of the young mice. **F** Representative Western blot (SDS) and analyses of levels of **G** 3RTau, **H** PHF1, **I** tTau, and **J** Ab from the soluble fraction of the aged mice. N = 3 for each age group *,** = $P < 0.05, 0.01$, respectively, when compared to non-tg control using one way ANOVA with Dunnett's post-hoc test. # = $P < 0.05$ when comparing the three lines of transgenic mice with one another using a one way ANOVA with Fisher's post-hoc test.

**Worsening neurodegenerative pathology in double transgenic APP-3RTau mice**

To investigate the neurodegenerative effects of combining overexpression of APP along with 3RTau we applied immunohistochemistry on sections with an antibody against the neuronal marker protein NeuN. In the young cohort, compared to the non-tg mice, the APP mice showed a trend of a decrease in neuronal density in the neocortex (Figure 7a ,b), dentate gyrus (Figure 7a, c), and region CA1 of the hippocampus (Figure 7a, d). The 3RTau mice displayed a lower level of immunoreactivity in the neocortex (Figure 7a, b), but similar neuronal density in the dentate gyrus (Figure 7a, c) and region CA1 of the hippocampus (Figure 7a, d). While the APP-3RTau mice showed the most significant loss of neuronal density in the neocortex (Figure 7a, b), dentate gyrus (figure 7a, c), and region CA1 of the hippocampus (Figure 7a, d).

In congruence with the young mice results, compared with the non-tg mice, the APP mice showed a mild relative loss of neurons in the dentate gyrus (Figure 7e, g), and region CA1 of the hippocampus (Figure 7e, h). The aged 3RTau mice showed decreased neuronal density in the three regions observed (Figure 7e, f-h). The APP-3RTau mice displayed even greater relative neuronal loss in the neocortex (Figure 7e, h), dentate gyrus (Figure 7e, g), and region CA1 of the hippocampus (Figure 7e, h). In summary, both ages of tg mice showed at least some level of relative neuronal loss in several regions, the most apparent was in the CA21 region of the hippocampus, especially for the APP-3RTau mice.

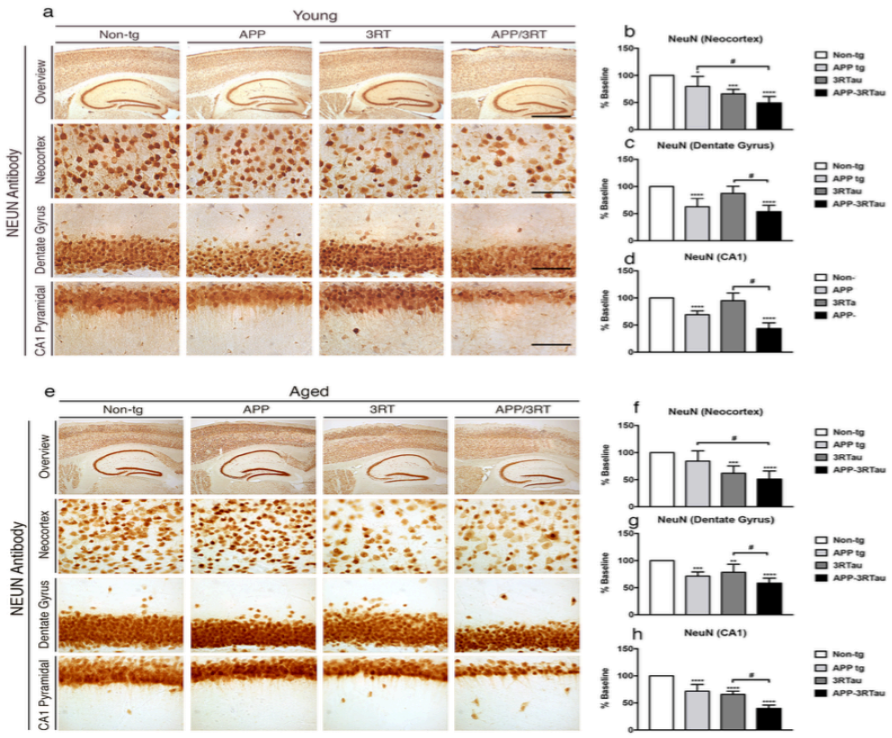


**Figure 7: Pattern of NEUN distribution in the brains of the three lines of mice compared with the non-tg control. A** Immunostaining with an antibody against NEUN was used on vibratome sections of the young mice, followed by analysis by digital bright field microscopy. Panels on the top row are low-magnification (40X) photomicrographs of the neocortex and hippocampus. The lower three rows of panels are higher magnification (630X) of the corresponding regions. **B** Image analysis of number of neuronal cells in the neocortex, **C** dentate gyrus, and **D** CA1 hippocampus region displaying NEUN distribution. **E** Immunostaining with an antibody against NEUN was used on vibratome sections of the aged mice, followed by analysis by digital bright field microscopy. Panels on the top row are low-magnification (40X) photomicrographs of the neocortex and hippocampus. The lower three rows of panels are higher magnification (630X) of the corresponding regions. **F** Image analysis of number of neuronal cells in the neocortex, **G** dentate gyrus, and **H** CA1 hippocampus region displaying NEUN distribution. *,**,***,**** = $P < 0.05, 0.01, 0.001, 0.0001$, respectively, when compared to non-tg control using one way ANOVA with Dunnett's post-hoc test. # = $P < 0.05$ when comparing the three lines of transgenic mice with one another using a one way ANOVA with Tukey-Kramer post-hoc test.

Analogous with these neuronal density results, immunohistochemical analysis for astrogliosis with an antibody against GFAP showed that in the young group the APP mice showed increased levels of GFAP than the non-tg mice in the neocortex (Figure 8a, b), dentate gyrus (Figure 8a, c) and CA1 of the hippocampus (Figure 8a, d). The young 3RTau mice did not showed significant astrogliosis in the neocortex (Figure 8a, b), the dentate gyrus (Figure 8a, c) or CA1 region of the hippocampus (Figure 8a, d). However, the young APP-3RTau tg mice displayed considerable astrogliosis in neocortex (Figure 8a, b), dentate gyrus (Figure 8a, c) and CA1 region of the hippocampus (Figure 8a, d).

For the aged cohort, the 3RTau and the APP tg mice showed mild astrogliosis in the neocortex (Figure 8e, f) and CA1 of the hippocampus (Figure 8e, h). In contrast, the APP-3RTau tg mice displayed significant astrogliosis in neocortex (Figure 8e, f), dentate gyrus (Figure 8e, g) and CA1 region of the hippocampus (Figure 8e, h). To summarize, these results support the conception that combining APP and 3RTau overexpression increases the vulnerability of pyramidal and granular neurons, most significantly in the CA1 region of the hippocampus.

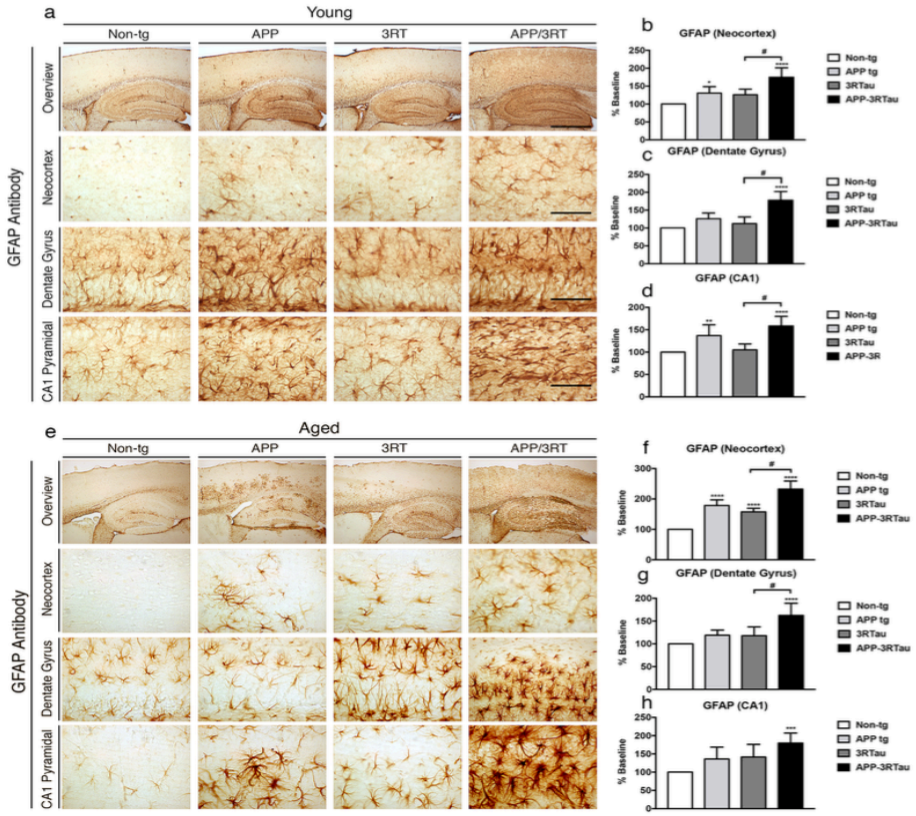


**Figure 8: Pattern of GFAP distribution in the brains of the three lines of mice compared with the non-tg control. A** Immunostaining with an antibody against GFAP was used on vibratome sections of the young mice, followed by analysis by digital bright field microscopy. Panels on the top row are low-magnification (40X) photomicrographs of the neocortex and hippocampus. The lower three rows of panels are higher magnification (630X) of the corresponding regions. **B** Image analysis of number of neuronal cells in the neocortex, **C** dentate gyrus, and **D** CA1 hippocampus region displaying GFAP distribution. **E** Immunostaining with an antibody against GFAP was used on vibratome sections of the aged mice, followed by analysis by digital bright field microscopy. Panels on the top row are low-magnification (40X) photomicrographs of the neocortex and hippocampus. The lower three rows of panels are higher magnification (630X) of the corresponding regions. **F** Image analysis of number of neuronal cells in the neocortex, **G** dentate gyrus, and **H** CA1 hippocampus region displaying GFAP distribution. *,**,***,**** = $P < 0.05, 0.01, 0.001, 0.0001$, respectively, when compared to non-tg control using one way ANOVA with Dunnett's post-hoc test. # = $P < 0.05$ when comparing the three lines of transgenic mice with one another using a one way ANOVA with Tukey-Kramer post-hoc test.

Again, I would like to thank Dr. Eliezer Masliah, for giving me this project and providing me with the lab equipment, reagents, and tissue needed to conduct the research of this project. I would like to extend my appreciation to Ed Rockenstein for engineering and providing me with the mice that were used for all of the data involved.

The Results Section is currently being prepared for submission for publication of the material as it appears in “Development of Biochemical Profile of Novel Bigenic Mouse AD Model”, Arner, Andrew; Adame, Adam. Andrew Arner was the primary investigator and author of this material.

## DISCUSSION

In the present study, we characterized the effects of short-term and long-term expression of mutant 3RTau gene with and without the presence of the hAPP gene in transgenic mice meant to model several neurodegenerative diseases, including PiD and AD. IHC data displayed that the mice carrying the mutant 3RTau gene showed extensive accumulation of 3RTau in the neocortex, dentate gyrus and area CA1 of the hippocampus, with increased levels observed in the bigenic mice. This pattern was also found when detecting for phosphorylated tau with both IHC and immunoblots. Elevated levels of glial scarring in IHC slides complemented these results in the transgenic mice, again with the highest levels found in the bigenic mice. As expected, given the aforementioned IHC patterns, neuronal density decreased in most areas, with the lowest densities found in the bigenic mice. Our immunoblot data only detected insoluble Aβ in the two lines of mice carrying the hAPP transgene; any within the soluble fraction was either present at levels below the threshold of observation or simply absent. This is consistent with other APP mouse models targeting Aβ plaques with SDS-containing buffers that detected Aβ predominantly in the insoluble fractions [13]. Given that abnormally high levels of NFTs are also present, increased levels of insoluble Aβ is consistent with AD pathology and evidence indicates a correlation with its presence and the onset and/or possibly the level of disease [14].

This paper aims to augment the initial results that observed the behavioral and biochemical properties of the novel mutant 3RTau (L266V and G272V mutations) tg mice, which are mutations associated with familial forms of PiD and found to develop results in mice consistent with patients suffering from the disease [15]. This is the first

study that examines the effects of having both transgenes present in a single line of mice. The interest in observing overexpression of 3RTau and hAPP comes from well-established evidence of synergy of the two proteins and the development of AD. The amyloid-cascade hypothesis claims that Aβ aggregation is central to AD pathology and increases the rate of neurodegeneration, while downstream tau aggregates elicit the actual pathogenic effects [16],[17]. As mentioned, our results appear consistent with this model given the higher levels of toxic phosphorylated tau and glial scarring, as well as the decreased neuronal density in the bigenic mice, compared with the 3RTau mice, and an even stronger trend compared with the non-tg mice. Our immunoblot data that correlates the concentration of some of the relevant tau kinases with the presence or absence of the transgenes of interest may elucidate at least a component that contributes to these differences.

There is a substantial amount of literature referencing that over-activation of the proline-directed serine/threonine kinases GSK3 and Cdk5 are significant components to the development of tauopathies [18]. Furthermore, evidence correlates GSK3 with both sporadic and familial forms of AD, not only because of its presence as a tau kinase, but also for its apparent upregulation of Aβ production from APP [19]. These preliminary results led to our focus on total levels of Cdk5 and GSK3. Further insight was sought by detecting levels of p35, the most effective full-length neuron specific activator of Cdk5 [20], as well as the state of GSK3β that has been shown to be its activated form, p-Y216 [21].

While our immunoblot results do not completely coincide with what established literature would suggest, there are several trends that do seem to conform. Total levels of

GSK3 were found to be higher in at least one, and often all three, of the transgenic mouse lines. In addition to this, higher levels of the activated form of GSK3β (p-Y216) were found in the soluble fraction of the two lines of young mice carrying the mutant 3RTau gene. This observation coupled with the significantly higher levels of p35 detected in the soluble fraction of the young bigenic mice parallels antecedent evidence mentioned above. This implies a potential early onset of tau and/or Aβ pathogenesis, which might explain at least a component of the toxic and neurodegenerative IHC and immunoblot results.

Taken together, our results suggest that expressing high levels of 3RTau as well as hAPP leads to neuropathology that resembles certain tauopathies such as PiD and AD. Because of this, the novel bigenic model characterized in this study may be used to further elucidate the disease progression of AD, as well as serve as a potential candidate for related pharmaceutical research.

## REFERENCES


1. Luc Buee, T.B., Valerie Buee-Scherrer, Andre Delacourte, Patrick R. Hoff, *Tau protein isoforms, phopshorylation and role in neurodegenerative disorders*. Elsevier, 2000. **33**: p. 95-130.

2. Hiroshi Takuma, S.A., Hiroshi Mori, *Isoforms changes of tau protein during development in various species*. Developmental Brain Research, 2003. **142**: p. 121-127.

3. Goode B. L., F.S.C., *Identification of a Novel Microtubule Binding and Assembly Domain in the Developmentally Regulated Inter-repeat Region of Tau*. Journal of Cell Biology, 1994. **124**: p. 769-782.

4. Goode B. L., C.M., Denis P., Feinstein S. C, *Structural and Functional Differences between 3-Repeat and 4-Repeat Tau Isoforms*. The Journal of Biological Chemistry, 2000. **49**: p. 38182-38189.

5. Gong C-X, I.K., *Hyperphosphorylation of Microtubule-Associated Protein Tau: A Promising Therapeutic Target for Alzheimer Disease*. Current Medicinal Chemistry, 2008. **15**(23): p. 2321-2328.

6. Khalid Iqbal, A.d.C.A., *Tau pathology in Alzheimer disease and other tauopathies*. Molecular Basis of Disease, 2005. **1739**(2): p. 198-210.

7. Iqbal K, L.F., Gong C-X, Grundke-Iqbal I, *Tau in Alzheimer Disease and Related Tauopathies*. Current Alzheimer research, 2010. **7**(8): p. 656-664.

8. Fei Liu, C.-X.G., *Tau exon 10 alternative splicing and tauopathies*. Molecular Neurodegeneration, 2008. **3**: p. 8.

9. Finder VH, G.R., *Amyloid-β Aggregation*. Neurodegenerative Diseases, 2007. **4**(1): p. 13-27.

10. Arriagada PV, G.J., *Neurofibrillary tangles but not semile plaques parallel duration and severity of Alzheimer's disease*. Neurology, 1992. **42**: p. 631-639.

11. Carillo-Mora P., L.R., Colin-Barenque L., *Amyloid Beta: Multiple Mechanisms of Toxicity and Only Some Protective Effects?* Oxidative Medicine and Cellular Longevity, 2014. **2014**.

12. Kumar D. K. V., C.S.H., Washicosky K., Eimer W., Tucker S., Ghofrani J., Lefkowitz A., McColl G., Goldstein L., Tanzi R., Moir R., *Amyloid-β peptide*

*protects against microbial infection in mouse and worm models of Alzheimer's disease*. Science Translational Medicine, 2016. **8**.

13. Philipson, O.e.a., *A highly insoluble state of Aβ similar to that of Alzheimer's disease brain is found in Arctic APP transgenic mice*. Neurobiology of Aging, 2009. **30**(9): p. 1393-1405.

14. Wang, J.e.a., *The Levels of Soluble versus Insoluble Brain Aβ Distinguish Alzheimer's Disease from Normal and Pathologic Aging*. Experimental Neurology, 1999. **158**(2): p. 328-337.

15. Edward Rockenstein, C.O., Kiren Ubhi, Michael Mante, Christina Patrick, Anthony Adame, Alejandro Bisquert, Margarita Trejo-Morales, Brian Spencer, Eliezer Masliah, *A Novel Triple repeat Mutant Tau Transgenic Model That Mimics Aspects of Pick's Disease and Fronto-temporal Tauopathies*. PLOS ONE, 2015. **10**(3).

16. Stancu, I.-C., *Models of β-amyloid induced Tau-pathology: the long and "folded" road to understand the mechanism*. Molecular Neurodegeneration, 2014. **9**(1): p. 1-14.

17. Karran, E., M. Mercken, and B.D. Strooper, *The amyloid cascade hypothesis for Alzheimer's disease: an appraisal for the development of therapeutics*. Nat Rev Drug Discov, 2011. **10**(9): p. 698-712.

18. Florian Plattner, M.A., K. Peter Giese, *The Roles of Cyclin-dependent Kinase 5 and Glycogen Synthase Kinase 3 in Tau Hyperphosphorylation*. The Journal of Biological Chemistry, 2006. **218**: p. 25457-25465.

19. Claudie Hooper, R.K., Simon Lovestone, *The GSK3 hypothesis of Alzheimer's disease*. Journal of Neurochemistry, 2008. **104**(6): p. 1433-1439.

20. Daqin Mao, P.H., *p35 is required for CDK5 Activation in Cellular Senescence*. Journal of Biological Chemistry, 2010. **285**(19): p. 14671-14680.

21. Takashi Ishizawa, N.S., Koichi Ishiguro, *Co-Localization of Glycogen Synthase Kinase-3 with Neurofibrillary Tangles and Granulovacuolar Degeneration in Transgenic Mice*. The American Journal of Pathology, 2003. **163**(3): p. 1057-1067.